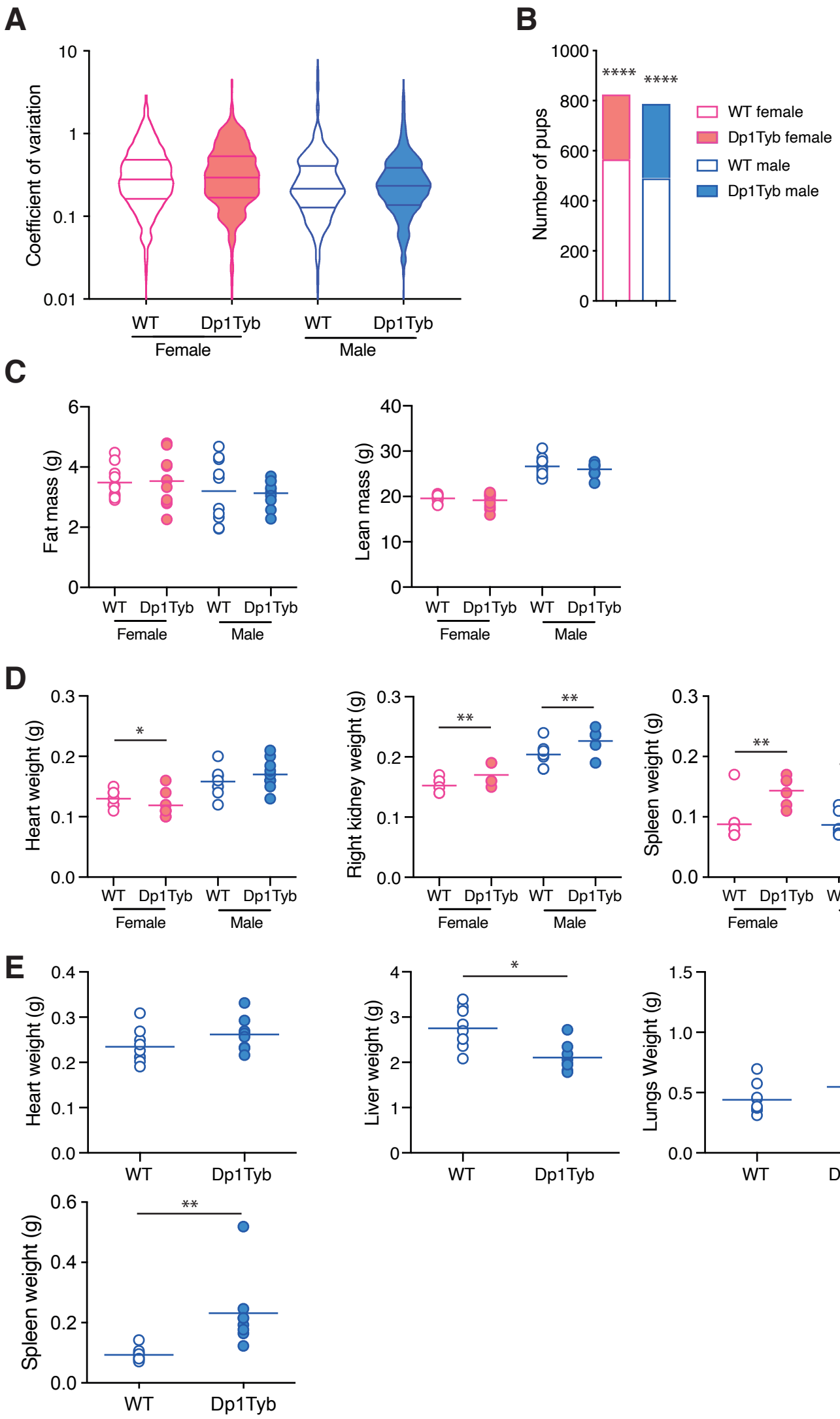
A
Coefficient of variation
10
1
0.1
0.01
WT
Dp1Tyb
WT
Dp1Tyb
Female
Male
B
Number of pups
1000
800
600
400
200
0
****
****
WT female
Dp1Tyb female
WT male
Dp1Tyb male
C
Fat mass (g)
6
4
2
0
Lean mass (g)
40
30
20
10
0
D
Heart weight (g)
0.3
0.2
0.1
0.0
*
Right kidney weight (g)
**
**
Spleen weight (g)
**
*
E
Heart weight (g)
Liver weight (g)
*
Lungs Weight (g)
1.5
1.0
0.5
0.0
Spleen weight (g)
0.6
0.4
0.2
0.0
**
WT
Dp1Tyb

Fig. S1. Decreased viability of Dp1Tyb mice. A, Coefficient of variation (standard deviation/mean) for all numerical parameters analysed shown as violin plots, with horizontal lines indicating median and 25th and 75th centiles. There are no significant differences between WT and Dp1Tyb measurements. Note the medians differ between females and males because some tests were carried out on only one sex (e.g. flow cytometric analysis was only carried out on females). **B**, Number of WT and Dp1Tyb mice recovered at weaning. **C**, Fat mass and lean mass of WT and Dp1Tyb mice (cohort 1) determined using ECHO-MRI. **D, E**, Weights of organs determined at 16 (D) and 57 (E) weeks of age. Horizontal lines indicate mean. * $0.01 < q < 0.05$; ** $0.001 < q < 0.01$; **** $q < 0.0001$.

Disease Models & Mechanisms • Supplementary information

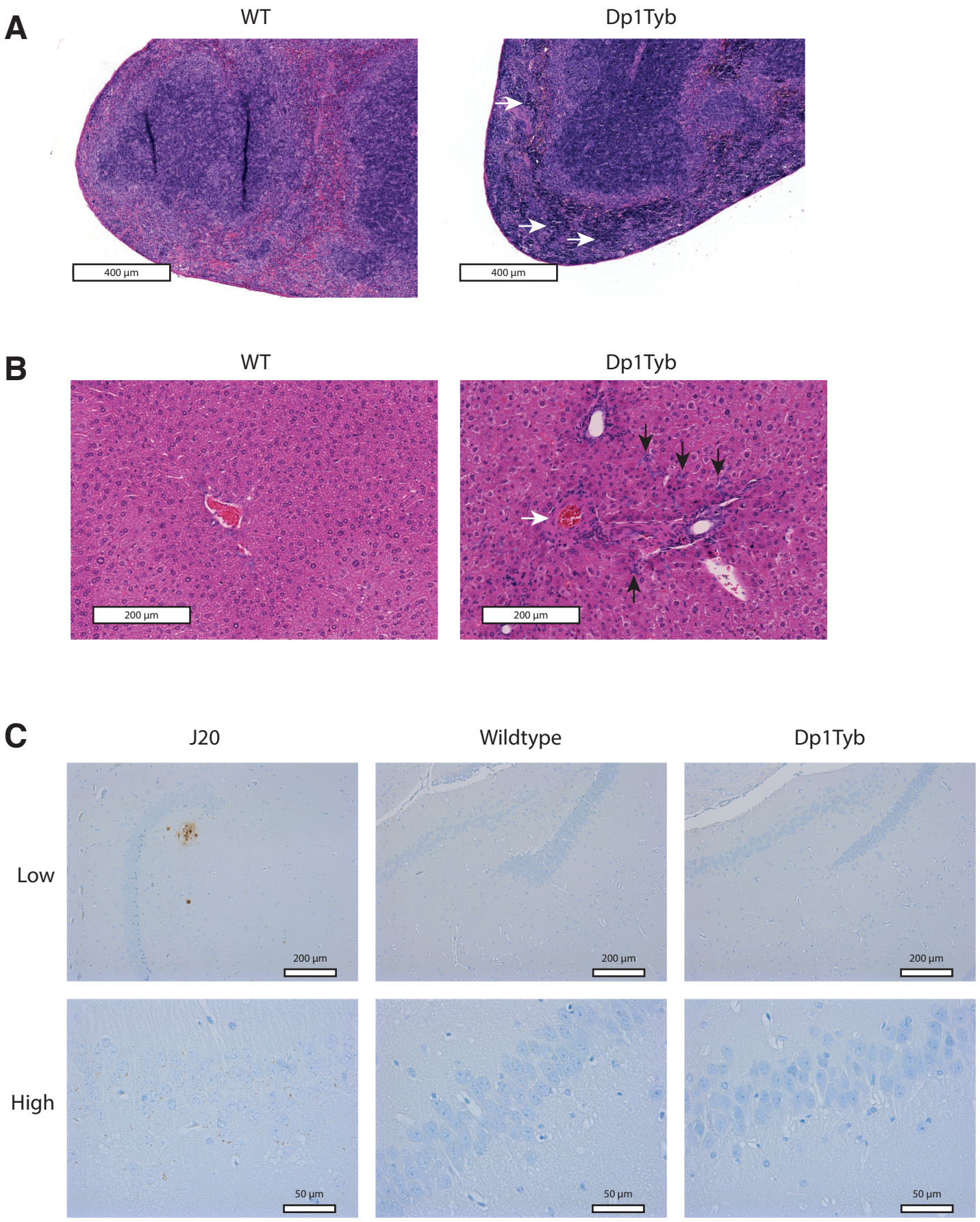

Fig. S2. Pathological changes in spleens and livers of Dp1Tyb mice. A, Sections of spleens from WT and Dp1Tyb mice (cohort 1) stained with haematoxylin and eosin showing increased extramedullary haematopoiesis in Dp1Tyb mice (white arrows). **B**, Sections of livers from WT and Dp1Tyb mice (cohort 1) stained with haematoxylin and eosin showing prominent vessels (white arrow) and bile duct hyperplasia in Dp1Tyb mice (black arrows). **C**, Immunohistochemistry staining of Aβ-positive extracellular plaques (brown) in the CA3/dentate gyrus region of the hippocampus of a 42-week old J20 mouse used as a positive control, and in 57-week old WT and Dp1Tyb mice. Images shown at low (10x) and high (40x) magnification. Intracellular Aβ-positive staining was evident in the J20 CA3 pyramidal neurons only; both WT and Dp1Tyb mice were negative for intracellular CA3 neuronal Aβ staining.

Disease Models & Mechanisms • Supplementary information

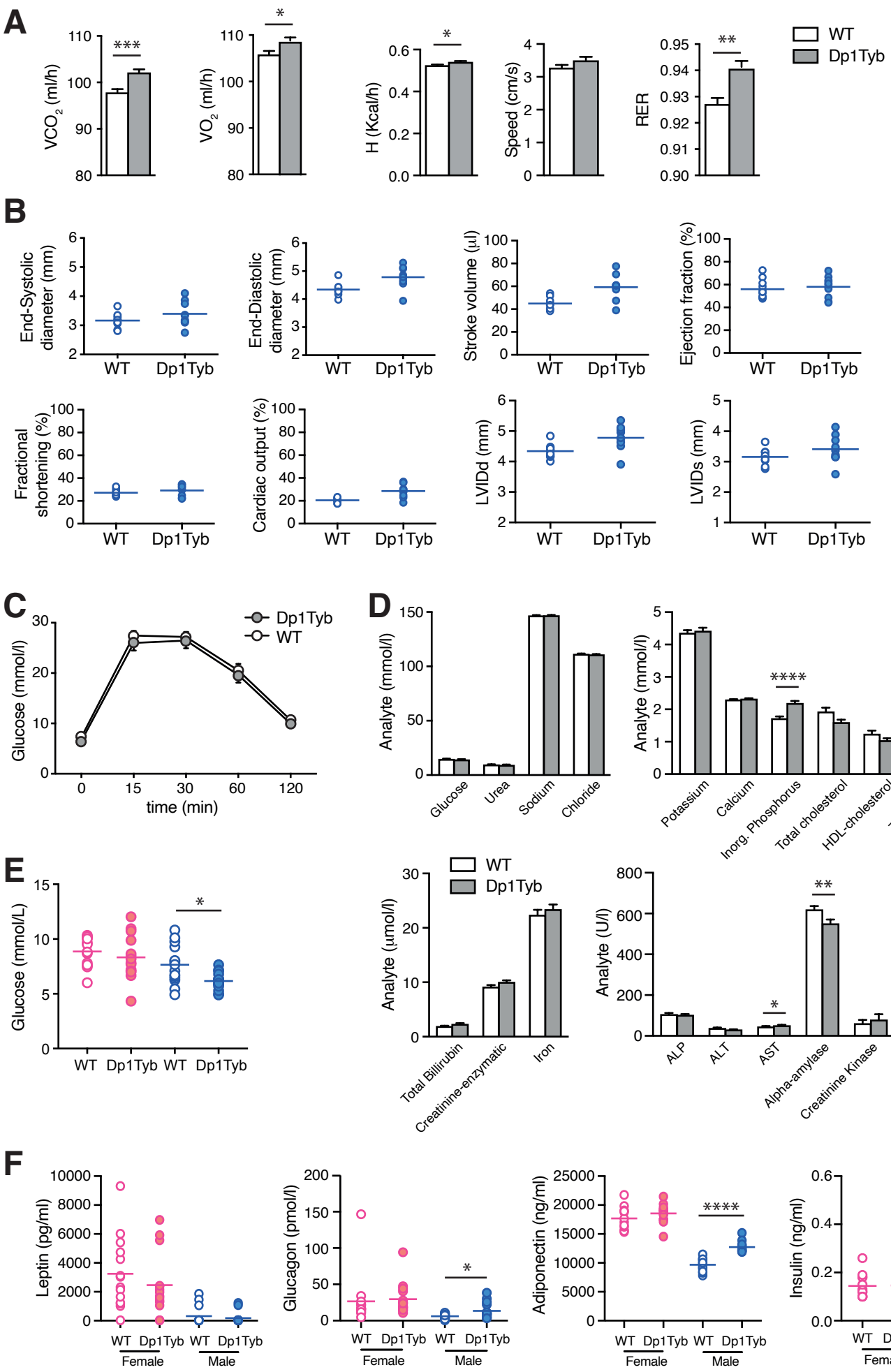

Fig. S3. Calorimetry, echocardiography, glucose tolerance and plasma clinical chemistry of Dp1Tyb mice. A, Mean±SEM CO_2 production (VCO_2), O_2 consumption (VO_2), heat production (H), movement speed and respiratory exchange ratio (RER) of WT and Dp1Tyb mice (cohort 1). **B**, End-systolic diameter, end-diastolic diameter, stroke volume, ejection fraction, fractional shortening, cardiac output, left ventricular inner diameter in diastole (LVIDd) and left ventricular inner diameter in systole (LVIDs) in WT and Dp1Tyb mice at 57 weeks of age (cohort 5) determined by echocardiography. Horizontal lines indicate mean. **C**, Mean±SEM blood glucose level in WT and Dp1Tyb mice (cohort 1) injected with 20% glucose solution. **D**, Mean±SEM concentrations of the indicated analytes in the blood of free-fed WT and Dp1Tyb mice (cohort 1). **E**, Levels of glucose in fasted WT and Dp1Tyb mice (cohort 2). **F**, Levels of the indicated hormones in the blood of fasted WT and Dp1Tyb mice (cohort 2). Horizontal lines indicate mean. * $0.01 < q < 0.05$; ** $0.001 < q < 0.01$; *** $0.0001 < q < 0.001$; **** $q < 0.0001$.

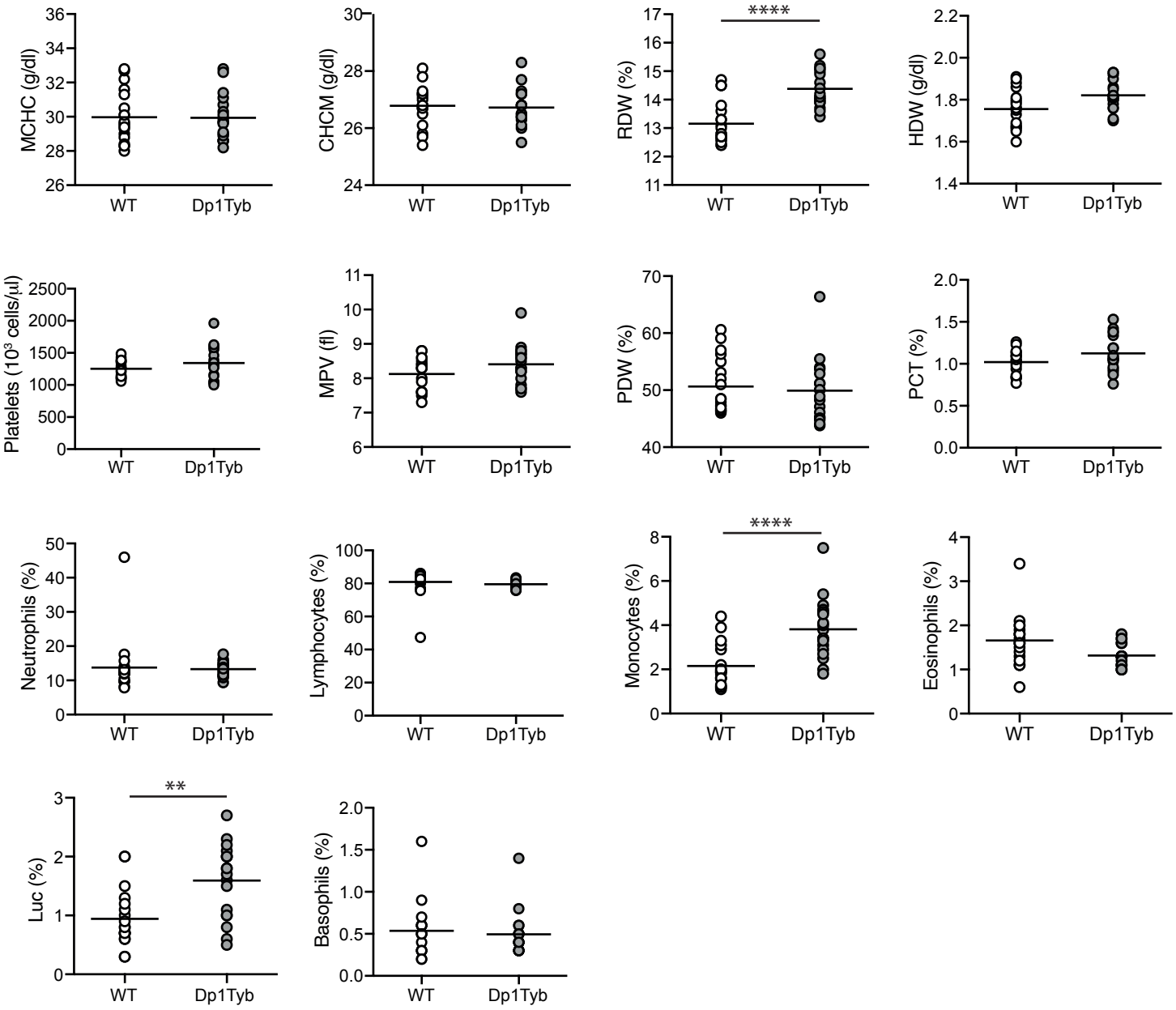

Fig. S4. Haematology of Dp1Tyb mice. Mean corpuscular haemoglobin concentration (MCHC), cell haemoglobin concentration mean (CHCM), red blood cell distribution width (RDW), haemoglobin distribution width (HDW), platelet concentration, mean platelet volume (MPV), platelet distribution width (PDW), plateletcrit (PCT), percentage of neutrophils, lymphocytes, monocytes, eosinophils, large unstained cells (Luc) and basophils in the blood of WT and Dp1Tyb mice (cohort 1). ** $0.001 < q < 0.01$; **** $q < 0.0001$.

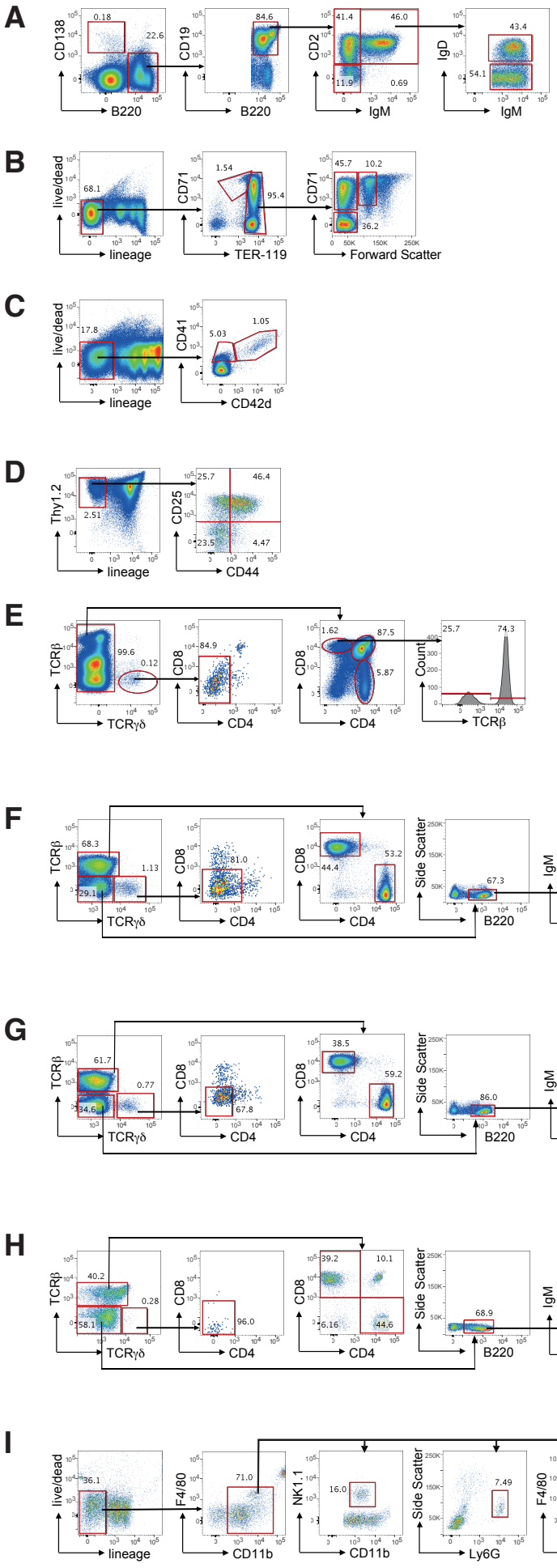

Bone Marrow

Thymus

Peripheral Lymph Nodes

Mesenteric Lymph Nodes

Blood

Fig. S5. Flow cytometric gating strategies for analysis of bone marrow, thymus, lymph nodes, and blood. Cell types were identified using the following gating strategies. **A-C**, Bone marrow. **A**, plasma cells ($B220^-CD138^+$), pro-B ($B220^+CD2^-IgM^-$), pre-B ($B220^+CD2^+IgM^-$), immature ($B220^+CD2^+IgM^+IgD^-$), mature ($B220^+CD2^+IgM^+IgD^+$) B cells. **B**, $Lineage^-$ cells ($B220^-CD3\varepsilon^-Mac\text{-}1^-Gr\text{-}1^-$) were subdivided into pro-erythroblasts (ProE, $CD71^+Ter119^{lo}$), EryA ($Ter119^{hi}CD71^+FSC^{hi}$), EryB ($Ter119^{hi}CD71^+FSC^{lo}$) and EryC ($Ter119^{hi}CD71^-FSC^{lo}$) erythroid progenitors. **C**, immature ($Lineage^-CD41^+CD42d^-$) and mature ($Lineage^-CD41^+CD42d^+$) megakaryoblasts. **D, E,** Thymus. **D**, Double negative (DN) thymocytes defined as $Lineage^-$ ($CD4^-CD8^-TCR\beta^-TCR\gamma\delta^-Gr\text{-}1^-CD11b^-CD11c^-Dx5^-Nk1.1^-B220^-$) and $Thy1.2^+$ were subdivided into DN1 ($CD44^+CD25^-$), DN2 ($CD44^+CD25^+$), DN3 ($CD44^-CD25^+$) and DN4 ($CD44^-CD25^-$). **E**, $TCR\gamma\delta$ thymocytes ($TCR\beta^-TCR\gamma\delta^+CD4^-CD8^-$), $TCR\gamma\delta^-$ cells were subdivided into double positive (DP, $CD4^+CD8^+$), $CD4^+$ single positives (SP, $CD4^+CD8^-$), $CD8^+$ intermediate single positives (ISP, $CD4^-CD8^+TCR\beta^-$), and $CD8^+$ SP ($CD4^-CD8^+TCR\beta^+$). **F-H,** Peripheral (F) and mesenteric (G) lymph nodes and blood (H). $\gamma\delta$ T cells ($TCR\beta^-TCR\gamma\delta^+CD4^-CD8^-$), $TCR\gamma\delta^-$ cells were subdivided into $CD4^+$ ($TCR\beta^+CD4^+CD8^-$) and $CD8^+$ ($TCR\beta^+CD4^-CD8^+$) T cells, B cells ($TCR\beta^-TCR\gamma\delta^-B220^+IgM^+IgD^+$). **I,** Blood. $Lineage^-$ cells ($B220^-CD4^-CD8^-$) were subdivided into NK cells ($CD11b^{lo}F4/80^-NK1.1^+$), neutrophils ($CD11b^{lo}F4/80^-Ly6G^+SSC^{hi}$), dendritic cells ($CD11b^{lo}F4/80^-CD11c^+$) and monocytes ($CD11b^{lo}F4/80^-CD11c^-Ly6C^+$). Numbers show percentage of cells falling into indicated gates.

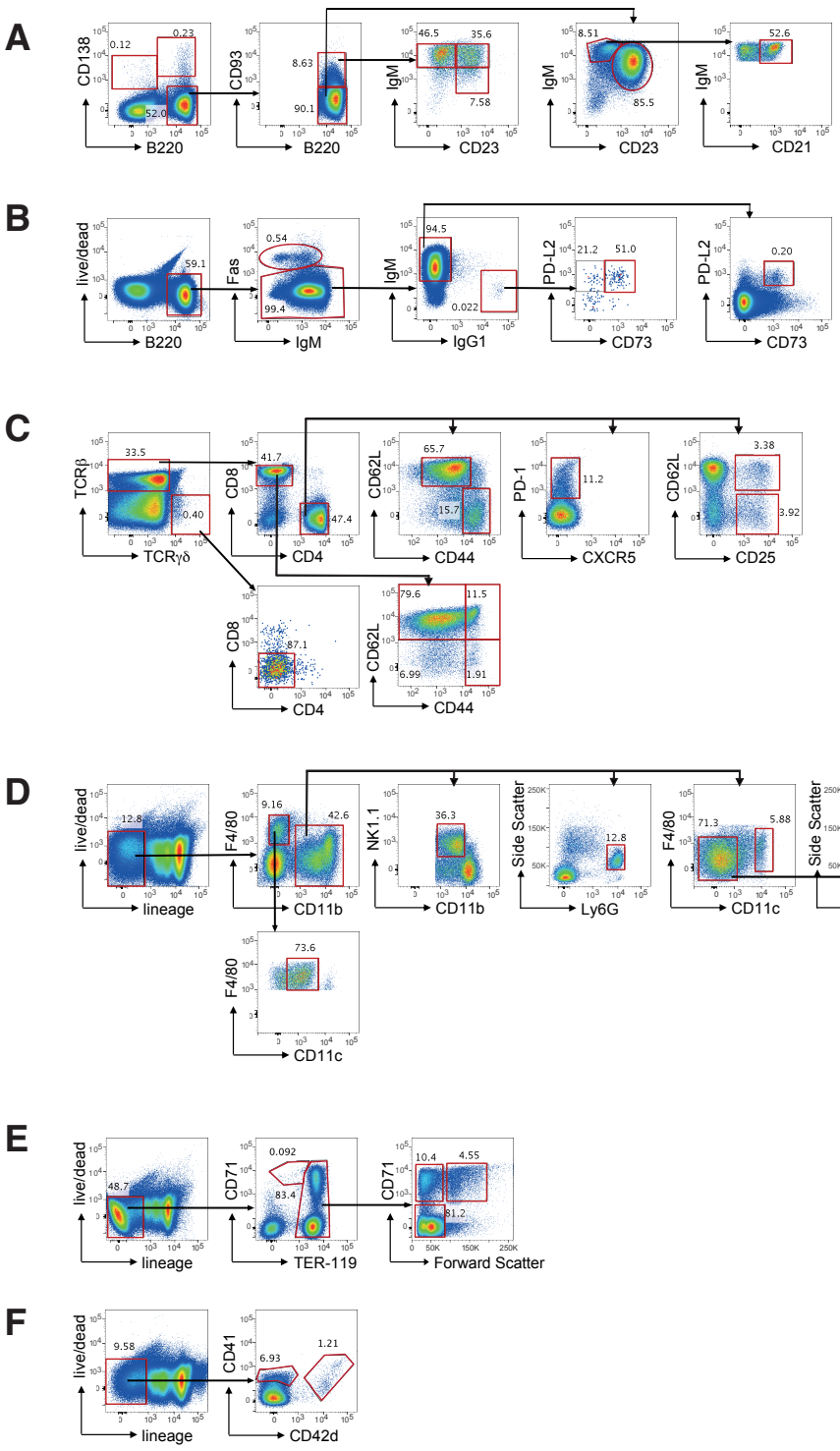

Spleen

Peritoneal Cavity

Fig. S6. Flow cytometric gating strategies for analysis of spleen and peritoneal cavity. Cell types were identified using the following gating strategies. **A-F,** Spleen. **A**, plasmablasts ($B220^{+}CD138^{+}$), plasma cells ($B220^{-}CD138^{+}$), transitional B cells ($B220^{+}CD93^{+}$) were subdivided into type 1 (T1, $IgM^{+}CD23^{-}$), T2 ($IgM^{+}CD23^{+}$) and T3 ($IgM^{lo}CD23^{+}$), mature B cells ($B220^{+}CD93^{-}$) were subdivided into follicular ($IgM^{+}CD23^{+}$) and marginal zone ($IgM^{+}CD23^{-}CD21^{+}$) B cells. **B**, Germinal centre (GC) B cells ($B220^{+}Fas^{+}$), IgM memory B cells (MBC) ($B220^{+}Fas^{-}IgM^{+}IgG1^{-}CD73^{+}PD\text{-}L2^{+}$) and IgG1 MBC ($B220^{+}Fas^{-}IgM^{-}IgG1^{+}CD73^{+}PD\text{-}L2^{+}$). **C**, γδ T cells ($TCR\beta^{-}TCR\gamma\delta^{+}CD4^{-}CD8^{-}$), $TCR\beta^{+}TCR\gamma\delta^{-}$ cells were subdivided into total ($CD4^{+}$), naïve ($CD4^{+}CD44^{lo}CD62L^{+}$) and effector ($CD4^{+}CD44^{hi}CD62L^{-}$) $CD4^{+}$ T cells, T follicular helper T cells ($CD4^{+}PD\text{-}1^{+}$), regulatory T cells ($CD4^{+}CD25^{+}CD62L^{+\ or\ -}$), total ($CD8^{+}$), naïve ($CD8^{+}CD44^{-}CD62L^{+}$), central memory ($CD8^{+}CD44^{+}CD62L^{+}$) and effector memory ($CD8^{+}CD44^{+}CD62L^{-}$) $CD8^{+}$ T cells. **D**, $Lineage^{-}$ cells ($B220^{-}CD3\varepsilon^{-}$) were subdivided into macrophages ($CD11b^{-}CD11c^{+}F4/80^{+}$), NK ($CD11b^{lo}F4/80^{-}NK1.1^{+}$), neutrophils ($CD11b^{+}F4/80^{-}Ly6G^{+}SSC^{hi}$), dendritic cells ($CD11b^{+}F4/80^{-}CD11c^{+}$) and monocytes ($CD11b^{+}F4/80^{-}CD11c^{-}$) subdivided into $Ly6C^{lo}$ and $Ly6C^{hi}$ cells. **E**, $Lineage^{-}$ cells ($B220^{-}CD3\varepsilon^{-}Mac\text{-}1^{-}Gr\text{-}1^{-}$) were subdivided into pro-erythroblasts (ProE, $CD71^{+}Ter119^{lo}$), EryA ($Ter119^{hi}CD71^{+}FSC^{hi}$), EryB ($Ter119^{hi}CD71^{+}FSC^{lo}$) and EryC ($Ter119^{hi}CD71^{-}FSC^{lo}$) erythroid progenitors. **F**, immature ($Lineage^{-}CD41^{+}CD42d^{-}$) and mature ($Lineage^{-}CD41^{+}CD42d^{+}$) megakaryoblasts. **G**, Peritoneal cavity. B1a ($B220^{+}CD5^{+}CD23^{-}$), B1b ($B220^{+}CD5^{-}CD23^{-}$) and B2 ($B220^{+}CD5^{-}CD23^{+}$) B cells and T cells ($B220^{-}CD5^{+}$). Numbers show percentage of cells falling into indicated gates.

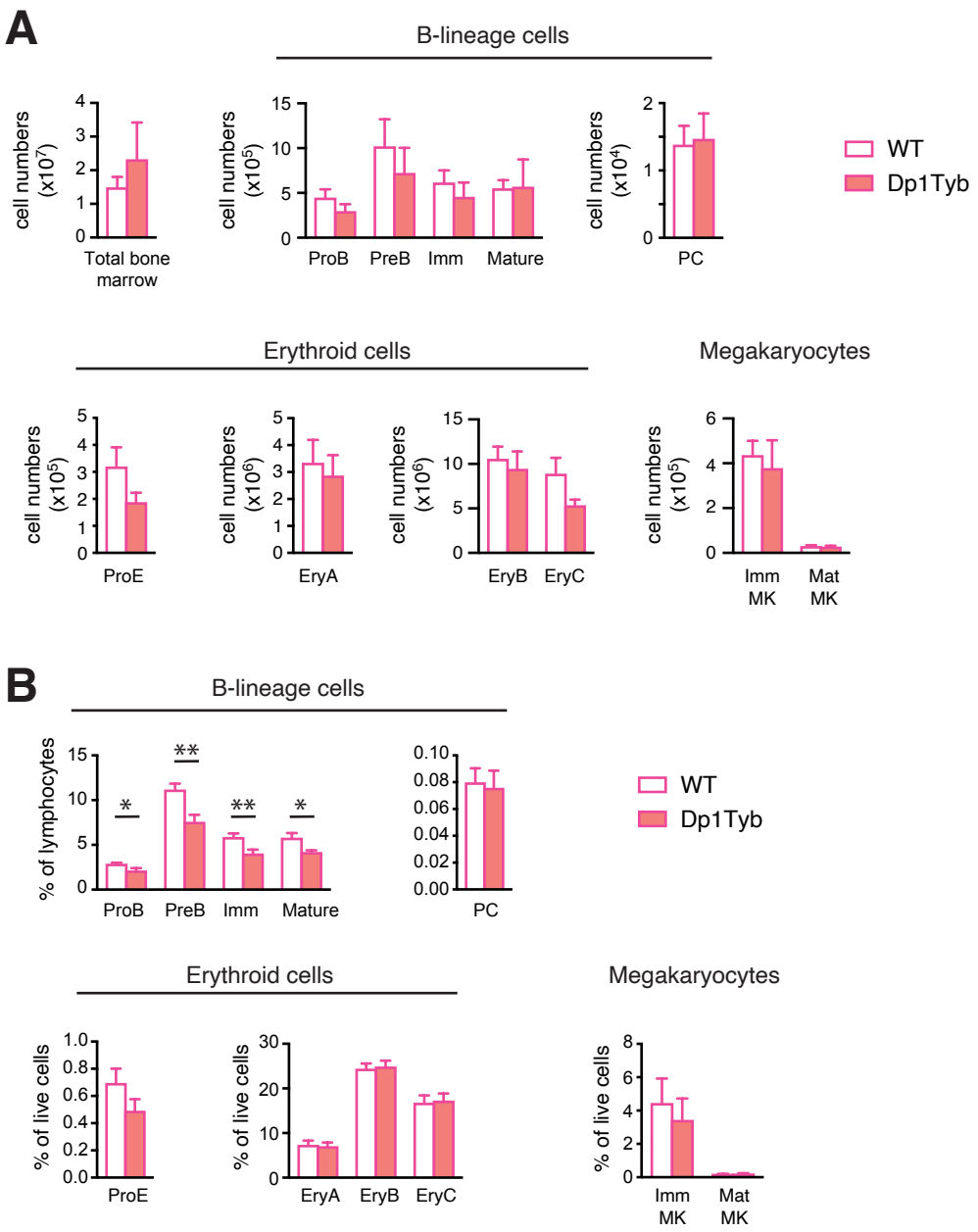

Fig. S7. Flow cytometric analysis of bone marrow cells in Dp1Tyb mice. A, Mean±SEM number of cells in the bone marrow of WT and Dp1Tyb mice (cohort 4) (2 tibia and 2 femurs/mouse), showing total cells, pro-B, pre-B, immature (Imm) and mature B cells, plasma cells (PC), pro-erythroblasts (ProE), EryA, EryB and EryC erythroid progenitors, and immature (Imm) and mature (Mat) megakaryoblasts (MK). **B**, Mean±SEM percentages of the populations shown in A. * $0.01 < q < 0.05$; ** $0.001 < q < 0.01$.

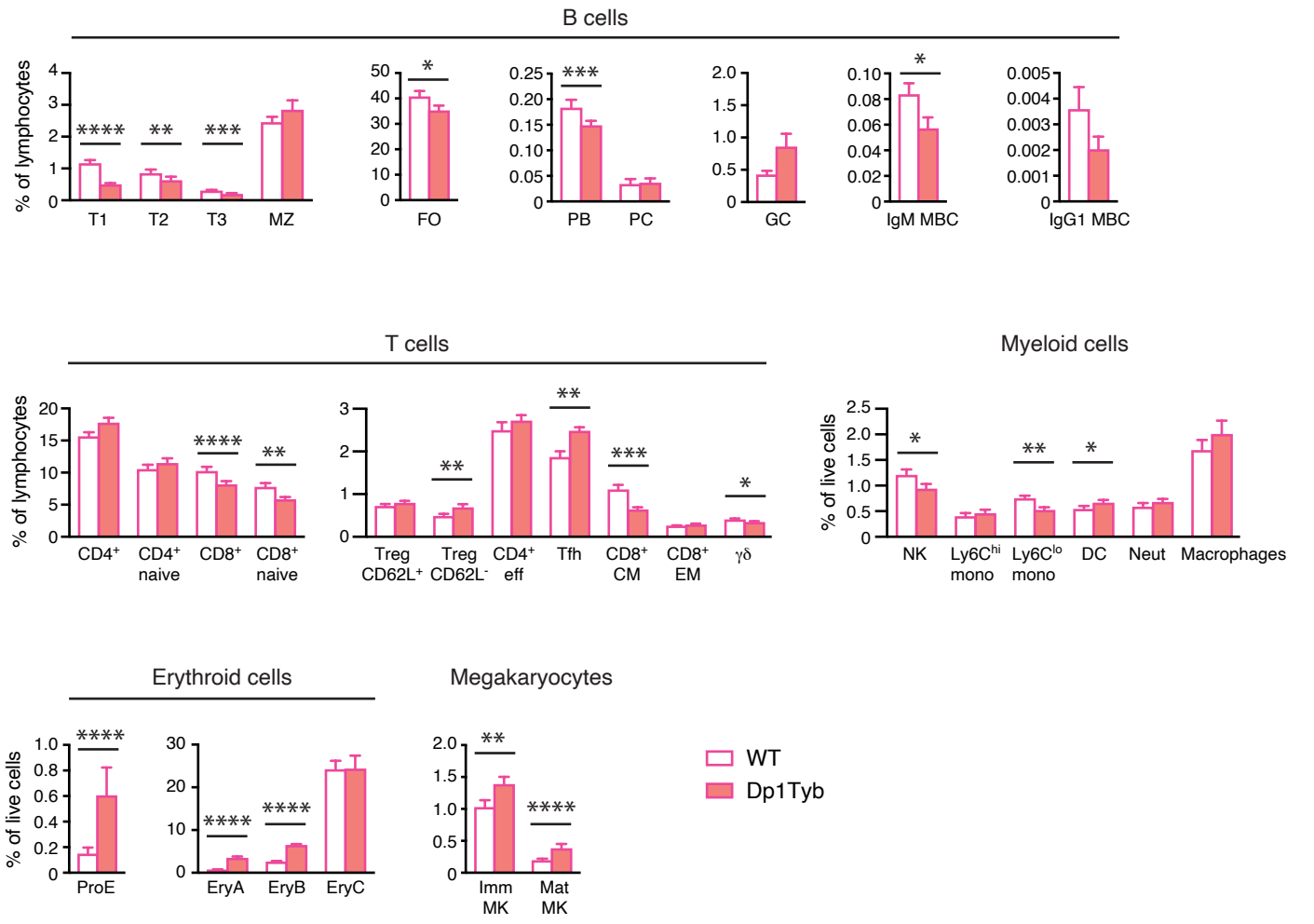

Fig. S8. Flow cytometric analysis of splenocytes in Dp1Tyb mice. Mean±SEM percentages of transitional type 1 (T1), T2, T3, marginal zone (MZ), follicular (FO), germinal centre (GC) B cells, plasmablasts (PB), plasma cells (PC), IgM and IgG1 memory B cells (MBC), and total or naive $CD4^+$ or $CD8^+$ T cells, $CD62L^+$ or $CD62L^-$ regulatory T cells (Treg), $CD4^+$ effector (eff) T cells, T follicular helper (Tfh) cells, $CD8^+$ central memory (CM) and effector memory (EM) T cells, γδ T cells, NK cells, $Ly6C^{hi}$ and $Ly6C^{lo}$ monocytes (mono), dendritic cells (DC), neutrophils (Neut), macrophages, pro-erythroblasts (ProE), EryA, EryB and EryC erythroid progenitors, and immature (Imm) and mature (Mat) megakaryoblasts (MK) in the spleen of WT and Dp1Tyb mice (cohort 4). * $0.01 < q < 0.05$; ** $0.001 < q < 0.01$; *** $0.0001 < q < 0.001$; **** $q < 0.0001$.

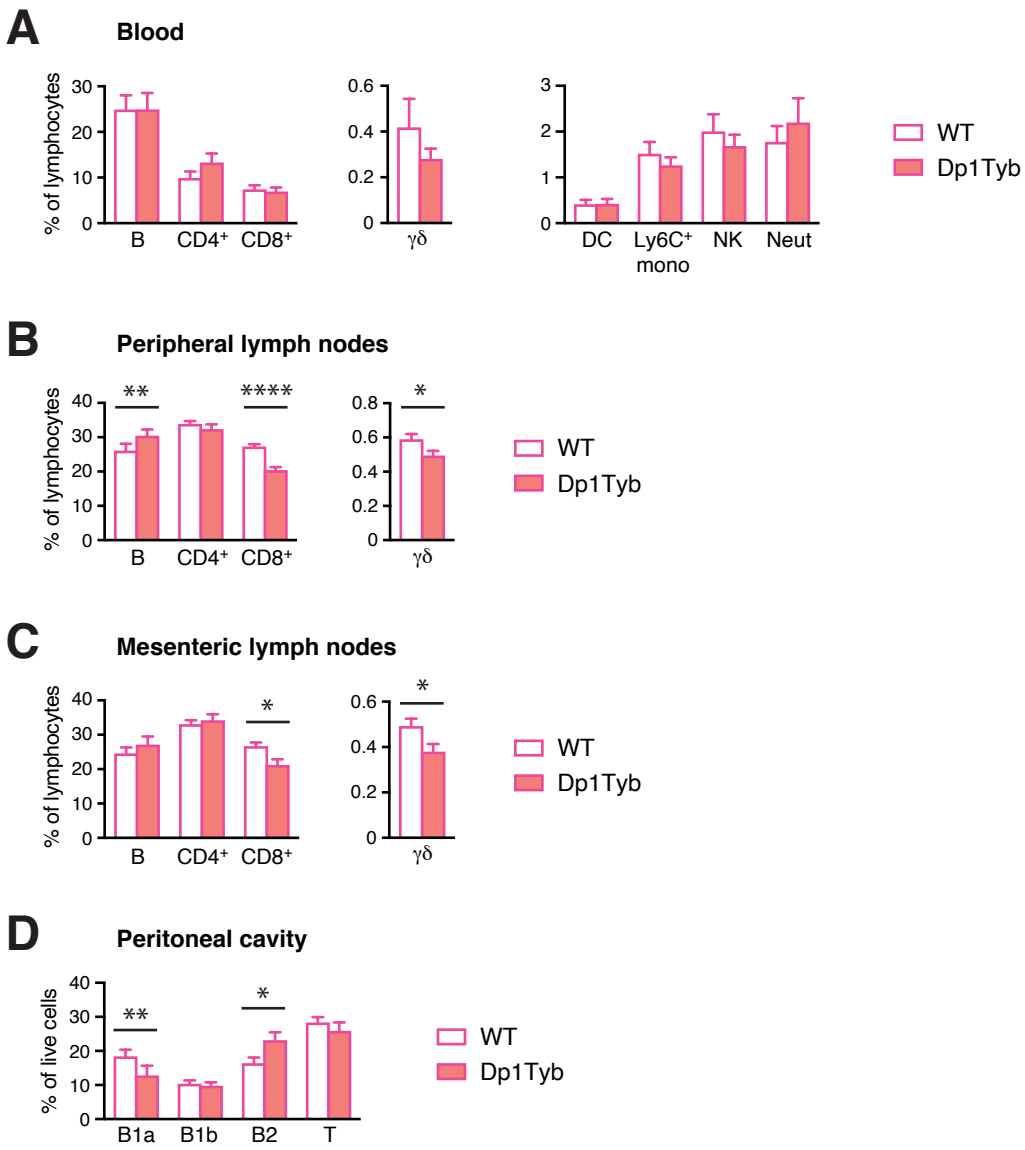

Fig. S9. Flow cytometric analysis of blood, lymph nodes and peritoneal cavity in Dp1Tyb mice. A-C, (**A**) Mean±SEM percentages of B cells, CD4$^+$, CD8$^+$ and γδ T cells, dendritic cells (DC), Ly6C$^+$ monocytes (mono), NK cells, and neutrophils (Neut) in the blood, (**B**) peripheral lymph nodes, and (**C**) mesenteric lymph nodes of WT and Dp1Tyb mice (cohort 4). **D**, Mean±SEM percentages of B1a, B1b and B2 B cells and T cells in the peritoneal cavity of WT and Dp1Tyb mice (cohort 4). * $0.01 < q < 0.05$; ** $0.001 < q < 0.01$; **** $q < 0.0001$.

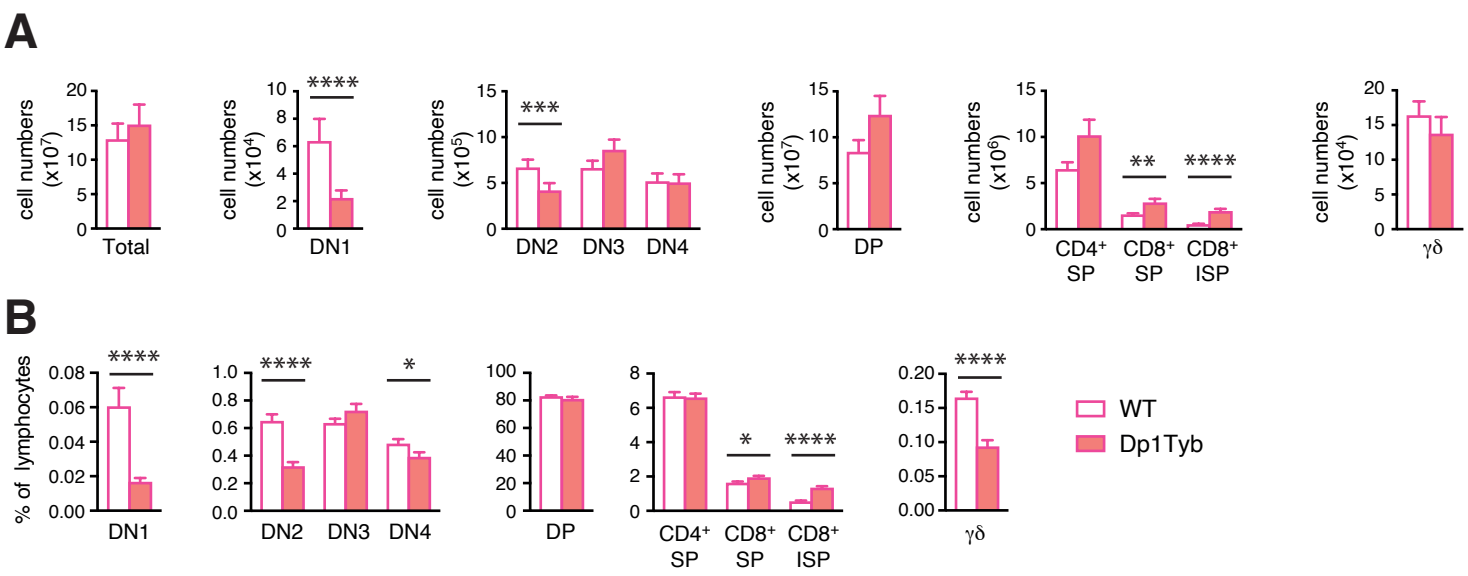

Fig. S10. Flow cytometric analysis of thymocytes in Dp1Tyb mice. A, Mean±SEM number of cells in the thymus of WT and Dp1Tyb mice (cohort 4), showing total cells, DN1, DN2, DN3, DN4, DP, CD4$^+$SP, CD8$^+$SP, CD8$^+$ISP and TCR$\gamma\delta^+$ thymocytes. **B**, Mean±SEM percentages of the populations shown in A. * $0.01 < q < 0.05$; ** $0.001 < q < 0.01$; *** $0.0001 < q < 0.001$; **** $q < 0.0001$.

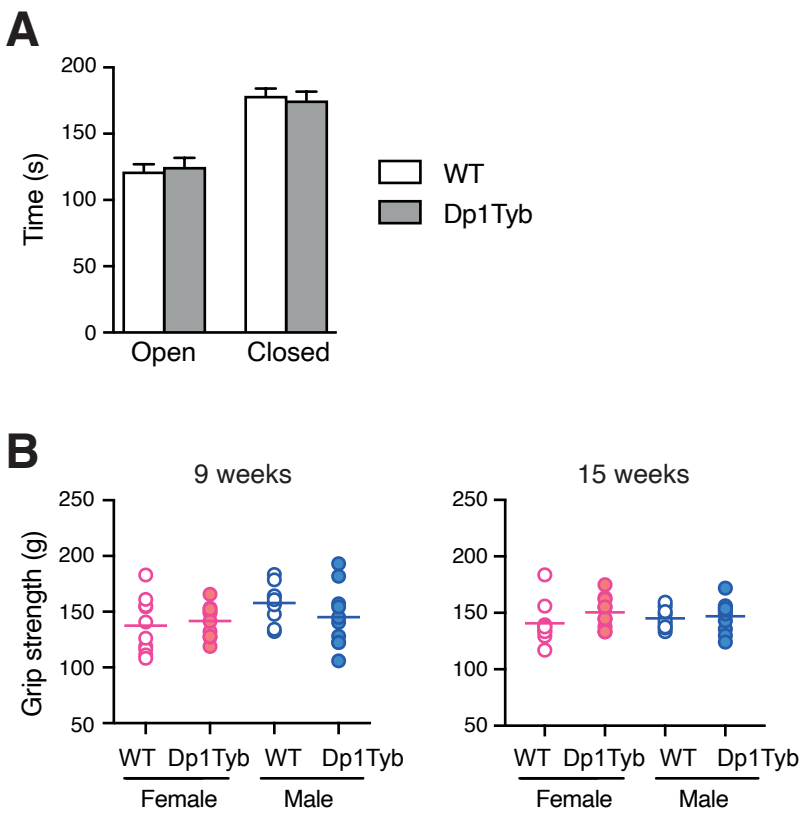

Fig. S11. Elevated zero maze and grip strength tests.

A, Mean±SEM time spent in the open and closed arms of an elevated zero maze by WT and Dp1Tyb mice (cohort 3). **B**, Grip strength of WT and Dp1Tyb mice (cohort 1) determined using all four limbs at 9 and 15 weeks of age. Horizontal lines indicate mean.

Disease Models & Mechanisms • Supplementary information

Table S1. Statistical Analysis.

Click here to download Table S1

Table S2. Dp1Tyb mice have abnormal heads, snouts, lips and gait. A, Table shows numbers of mice that gave the expected or not expected result in each of the tests in the Combined SHIRPA and Dysmorphology (CSD) tests. Dp1Tyb and WT mice were tested at 9 and 15 weeks of age (cohort 1). Test showing statistically significant differences ($q<0.05$) between Dp1Tyb and WT mice at either 9 or 15 weeks or both are highlighted in yellow. **B,** Locomotor activity measured as mean±sem number of squares entered by the mouse in 30s.

A

	9 weeks				15 weeks				
	WT		Dp1Tyb		WT		Dp1Tyb		
Test	**As expected**	**Not as expected**	**As expected**	**Not as expected**	**As expected**	**Not as expected**	**As expected**	**Not as expected**	**Comments**
Tail	19	1	14	6	17	4	10	10	
Coat	20	0	20	0	21	0	20	0	
Forelimbs	20	0	20	0	21	0	20	0	
Hindlimbs	20	0	20	0	21	0	20	0	
Vibrissae	19	1	20	0	21	0	20	0	
Head	18	2	11	9	19	2	8	12	Abnormal shape
Ears	20	0	20	0	21	0	20	0	
Snout Size	20	0	9	11	20	1	13	7	Decreased
Activity (body position)	19	1	17	3	21	0	18	2	
Tremor	20	0	17	3	3	18	14	6	Tremor present
Faecal pellet	19	0	20	0	21	0	20	0	
Feet position in jar	20	0	16	4	21	0	20	0	
Transfer Arousal	20	0	18	2	21	0	18	2	
Gait	20	0	14	6	20	1	6	14	Lack of fluid movement
Tail Elevation	20	0	20	0	21	0	20	0	
Startle Response	10	0	9	1	20	1	14	6	
Trunk Curl	20	0	19	1	21	0	20	0	
Limb Grasp	20	0	17	3	21	0	19	1	
Visual Placing	10	0	20	0	21	0	20	0	
Body Tone	20	0	20	0	21	0	17	3	
Limb Tone	20	0	17	0	16	5	14	6	
Paws	20	0	20	0	21	0	20	0	
Digits	20	0	20	0	21	0	20	0	
Nail	17	3	20	0	21	0	20	0	
Skin	20	0	20	0	21	0	20	0	
Teeth	20	0	20	0	21	0	20	0	
Genitalia	20	0	20	0	21	0	20	0	
Mouth Morphology	20	0	18	2	21	0	20	0	
Lip Morphology	18	2	6	14	21	0	19	1	Abnormal shape
Salivation	20	0	20	0	21	0	20	0	
Contact Righting	20	0	20	0	20	1	20	0	
Negative Geotaxis	20	0	16	4	21	0	17	3	
Vocalization	18	2	20	0	21	0	20	0	
Aggression	17	3	20	0	20	1	20	0	
Head Bobbing	20	0	20	0	21	0	20	0	

B

	9 weeks		15 weeks	
	WT	**Dp1Tyb**	**WT**	**Dp1Tyb**
Locomotor Activity (Mean±sem)	26.55±1.07	30.15±1.86	20.45±1.23	22.38±2.53

Disease Models & Mechanisms • Supplementary information

Table S3. Dp1Tyb mice have abnormally shaped heads. Table shows numbers of Dp1Tyb and WT mice that were assessed as being normal or abnormal for each of the features listed from X-ray analysis of mice tested at 14 weeks of age (cohort 1). Test showing statistically significant differences ($q<0.05$) between Dp1Tyb and WT mice is highlighted in yellow.

	WT		Dp1Tyb		
	Normal	**Abnormal**	**Normal**	**Abnormal**	**Comments**
Skull shape	19	1	0	20	Abnormal shape
Zygomatic bone	19	1	19	1	
Maxilla	19	1	13	7	
Clavicle	20	0	20	0	
Scapulae	20	0	20	0	
Humerus shape	20	0	20	0	
Fusion of ribs	20	0	20	0	
Shape of ribs	20	0	20	0	
Vertebrae shape	19	0	19	0	
Fused vertebrae	19	1	19	1	
Processes on vertebrae	20	0	20	0	
Joints	20	0	20	0	
Syndactylism	20	0	20	0	
Brachydactyly	20	0	20	0	
Digit integrity	20	0	20	0	
Pelvis	18	2	16	4	
Femur shape	20	0	20	0	
Fibula	20	0	20	0	
Tibia	20	0	20	0	
Radius	20	0	20	0	
Ulna	20	0	20	0	
Mandibles	19	1	20	0	
Teeth	19	1	19	0	

Disease Models & Mechanisms • Supplementary information

Table S4. Dp1Tyb mice have increased splenic extramedullary haematopoiesis, portal tract anomalies in the liver and otitis media. Table shows incidence of tissues with an appearance considered microscopically within normal limits and tissues where pathological findings are present. Pathological findings may be spontaneous background lesions expected in the strain of mouse or considered specific to the genotype of the animals. Pathological analysis on WT and Dp1Tyb mice in cohort 1 was carried out at 16 weeks of age. Significant findings (different from variations in spontaneous C57BL/6J background pathology) in Dp1Tyb mice were increased splenic extramedullary haematopoiesis, portal tract anomalies in the liver and otitis media. These are highlighted in yellow.

	Females				Males				
	WT		Dp1Tyb		WT		Dp1Tyb		
Tissue	Within normal limits	Pathological findings present	Within normal limits	Pathological findings present	Within normal limits	Pathological findings present	Within normal limits	Pathological findings present	Comments
Salivary gland	4	0	3	1	2	2	5	0	
Lungs	2	2	1	3	4	0	2	3	Increased perivascular inflammation in Dp1Tyb mice but considered within normal variation in background mouse strain.
Thyroid	4	0	4	0	4	0	5	0	
Trachea	4	0	4	0	4	0	4	1	
Parathyroid	2	0	2	0	3	0	2	0	
Kidney	0	4	0	4	2	2	0	5	Pelvic dilatation and inflammatory cell infiltrates seen in both genotypes. Significance uncertain but considered within normal variation in background mouse strain.
Heart	4	0	4	0	4	0	5	0	
Tongue	4	0	4	0	4	0	5	0	
Adrenal	1	3	1	3	3	1	2	3	Subcapsular cell hyperplasia in both genotypes but considered within normal variation in background mouse strain.
Liver	0	4	0	7	3	1	0	4	Significant lesion. Bile duct hyperplasia and prominent portal vasculature increased in Dp1Tyb mice. Not seen spontaneously.
Pancreas	4	0	5	2	4	0	3	1	Fatty atrophy and inflammatory cell foci in Dp1Tyb mice but considered within normal variation in background mouse strain.
Gall bladder	3	0	6	0	3	1	2	2	
Spleen	0	4	0	7	0	4	0	4	Significant lesion. Extramedullary haematopoiesis increased in Dp1Tyb mice.
Thymus	3	1	5	2	4	0	3	1	
Mesenteric lymph node	3	0	2	0	3	0	3	0	
Oesophagus	3	1	4	0	4	0	4	0	
Duodenum	3	0	3	0	4	0	4	0	
Jejunum	4	0	4	0	4	0	4	0	
Ileum	4	0	4	0	4	0	4	0	
Colon	3	1	4	0	4	0	4	0	
Caecum	4	0	4	0	4	0	4	0	
Stomach	4	0	4	0	4	0	4	0	
Bladder	3	0	4	0	4	0	4	0	
Skin	4	0	4	0	4	0	4	0	
Muscle	4	0	4	0	4	0	4	0	
Eye	4	0	4	0	3	1	4	0	
Brain	3	1	2	2	4	0	3	1	Ventricular dilatation more frequent in Dp1Tyb mice but considered within normal variation in background mouse strain.
Spinal cord	4	0	4	0	4	0	4	0	
Pituitary	4	0	4	0	3	1	3	1	
Sciatic nerve	4	0	4	0	4	0	4	0	
Femur	4	0	4	0	4	0	4	0	
Sternum	4	0	4	0	4	0	3	0	
Nasal cavity	3	1	3	1	4	0	4	0	
Harderian gland	0	0	0	0	4	0	4	0	
Ear	0	0	0	2	4	0	0	4	Significant lesion. Otitis media in Dp1Tyb mice.
Uterus	4	0	4	0					
Ovary	4	0	4	0					
Testes					1	3	1	3	Tubular atrophy in both genotypes but considered within normal variation in background mouse strain.
Seminal vesicles					3	1	4	0	
Epididymides					4	0	4	0	
Prostate					4	0	4	0	

Disease Models & Mechanisms • Supplementary information

Table S5. No significant eye abnormalities in Dp1Tyb mice. Table shows numbers of Dp1Tyb and WT mice that were assessed as being normal or abnormal for each of the features or pathologies listed following eye examination at 15 weeks of age (cohort 1). There were no significant differences between Dp1Tyb and WT mice.

	WT		Dp1Tyb	
	Normal	**Abnormal**	**Normal**	**Abnormal**
eye	19	1	18	0
bulging eye	19	0	18	0
eye haemorrhage	19	0	18	0
eyelid morphology	19	0	18	0
eyelid closure	19	0	18	0
narrow eye opening	19	0	18	0
cornea	19	0	18	0
corneal opacity	18	2	17	1
corneal vascularization	19	0	18	0
iris/pupil	18	0	18	0
pupil position	18	0	18	0
pupil shape	18	0	18	0
pupil dilation	18	0	18	0
pupil light response	18	0	18	0
iris pigmentation	18	0	18	0
lens	18	0	18	0
lens opacity	18	1	16	2
fusion between cornea & lens	18	0	18	0
synechia	18	0	18	0
retina	18	0	18	0
retinal pigmentation	18	0	18	0
retinal structure	18	0	18	0
optic disc	18	0	18	0
retinal blood vessels	18	0	17	1
retinal blood vessels structure	18	0	18	0
retinal blood vessels pattern	18	0	16	2
persistence of hyaloid vascular system	15	3	18	0

Table S6. Comparison of phenotypes between human DS and Dp1Tyb and Dp1Yey mouse models of DS. Table shows phenotypes seen in human DS and results of related phenotypic analysis in Dp1Tyb and Dp1Yey mice. Orange boxes indicate where the results of the mouse phenotyping are different to human studies, blue boxes for differences between Dp1Tyb and Dp1Yey mice. ND, not determined.

Human DS		Dp1Tyb mice		Dp1Yey mice	
Phenotype	**Reference**	**Phenotype**	**Reference**	**Phenotype**	**Reference**
Learning and memory deficits	(Grieco et al., 2015; Lott and Dierssen, 2010)	Learning and memory deficits, and electrophysiological alterations	This study and (Chang et al., 2020)	Learning and memory deficits, and electrophysiological alterations	(Aziz et al., 2018; Goodliffe et al., 2016; Jiang et al., 2015; Nguyen et al., 2018; Pinto et al., 2020; Raveau et al., 2018; Souchet et al., 2019; Yu et al., 2010a; Zhang et al., 2014)
Locomotor deficits	(Cardoso et al., 2015; Malak et al., 2015)	Locomotor deficits	This study	Locomotor deficits	(Aziz et al., 2018; Goodliffe et al., 2016; Watson-Scales et al., 2018)
Impaired sympathetic innervation	(Fernhall and Otterstetter, 2003; Iellamo et al., 2005)	ND		Impaired sympathetic innervation	(Patel et al., 2015)
Disrupted sleep	(Grieco et al., 2015)	Disrupted sleep	This study	Disrupted sleep	(Levenga et al., 2018)
Alzheimer's disease	(Wiseman et al., 2015)	No amyloid deposition	This study	ND	
Congenital heart defects	(Vis et al., 2009)	Congenital heart defects	(Lana-Elola et al., 2016)	Congenital heart defects	(Li et al., 2007; Liu et al., 2011)
Craniofacial alterations	(Vicente et al., 2020)	Craniofacial alterations	This study and (Toussaint et al., 2021)	Craniofacial alterations	(Starbuck et al., 2014; Takahashi et al., 2020)
Decreased stature	(Korenberg et al., 1994; LaCombe and Roper, 2020)	Reduced length of body, tibia and femur	This study and (Thomas et al., 2020)	ND	
Decreased bone mineral density	(Baptista et al., 2005; Costa et al., 2018; LaCombe and Roper, 2020)	Decreased bone mineral density	This study and (Thomas et al., 2020)	ND	
Increased body fat	(Gutierrez-Hervas et al., 2020)	No change in lean mass or fat mass	This study	No change in lean mass or fat mass	(Menzies et al., 2021)
Increased rates of type 1 and type 2 diabetes	(Alexander et al., 2016; Johnson et al., 2019)	Decreased blood glucose in fasting mice	This study	Elevated blood glucose in fasting mice	(Peiris et al., 2016)
		Pre-diabetic state	This study	ND	
Transient abnormal myelopoiesis	(Bhatnagar et al., 2016; Garnett et al., 2020)	Increased megakaryocyte-erythrocyte progenitors	This study	Increased megakaryocyte-erythrocyte progenitors	(Liu et al., 2018)
		Macrocytic anaemia, splenomegaly	This study	ND	
Increased type I interferon response	(Sullivan et al., 2016)	ND		Increased type I interferon response	(Sullivan et al., 2016)
Hearing deficits	(Kreicher et al., 2018)	Hearing deficits	This study	Hearing deficits	(Bhutta et al., 2013)
Altered eye structures (eyelid, iris, cornea, lens, retina)	(Krinsky-McHale et al., 2014)	No changes found	This study	ND	
Increased retinal thickness	(Laguna et al., 2013)	ND		Increased retinal thickness	(Victorino et al., 2020)
Reduced VO_2, VCO_2, breathing rate, RER	(Allison et al., 1995; Boonman et al., 2019; Luke et al., 1994)	Higher VO_2, VCO_2, breathing rate, and RER	This study	Higher VO_2, VCO_2	(Menzies et al., 2021)
Muscle hypotonia		Normal grip strength	This study	ND	
Placental abnormalities	(Adams et al., 2020)	ND		Placental abnormalities	(Adams et al., 2021)

REFERENCES

Adams, A. D., Guedj, F. and Bianchi, D. W. (2020). Placental development and function in trisomy 21 and mouse models of Down syndrome: Clues for studying mechanisms underlying atypical development. *Placenta* **89**, 58-66.

Adams, A. D., Hoffmann, V., Koehly, L., Guedj, F. and Bianchi, D. W. (2021). Novel insights from fetal and placental phenotyping in 3 mouse models of Down syndrome. *Am J Obstet Gynecol*.

Alexander, M., Petri, H., Ding, Y., Wandel, C., Khwaja, O. and Foskett, N. (2016). Morbidity and medication in a large population of individuals with Down syndrome compared to the general population. *Dev Med Child Neurol* **58**, 246-254.

Allison, D. B., Gomez, J. E., Heshka, S., Babbitt, R. L., Geliebter, A., Kreibich, K. and Heymsfield, S. B. (1995). Decreased resting metabolic rate among persons with Down Syndrome. *Int J Obes Relat Metab Disord* **19**, 858-861.

Aziz, N. M., Guedj, F., Pennings, J. L. A., Olmos-Serrano, J. L., Siegel, A., Haydar, T. F. and Bianchi, D. W. (2018). Lifespan analysis of brain development, gene expression and behavioral phenotypes in the Ts1Cje, Ts65Dn and Dp(16)1/Yey mouse models of Down syndrome. *Dis Model Mech* **11**.

Baptista, F., Varela, A. and Sardinha, L. B. (2005). Bone mineral mass in males and females with and without Down syndrome. *Osteoporos Int* **16**, 380-388.

Bhatnagar, N., Nizery, L., Tunstall, O., Vyas, P. and Roberts, I. (2016). Transient Abnormal Myelopoiesis and AML in Down Syndrome: an Update. *Curr Hematol Malig Rep* **11**, 333-341.

Bhutta, M. F., Cheeseman, M. T., Herault, Y., Yu, Y. E. and Brown, S. D. (2013). Surveying the Down syndrome mouse model resource identifies critical regions responsible for chronic otitis media. *Mamm Genome* **24**, 439-445.

Boonman, A. J. N., Schroeder, E. C., Hopman, M. T. E., Fernhall, B. O. and Hilgenkamp, T. I. M. (2019). Cardiopulmonary Profile of Individuals with Intellectual Disability. *Med Sci Sports Exerc* **51**, 1802-1808.

Cardoso, A. C., Campos, A. C., Santos, M. M., Santos, D. C. and Rocha, N. A. (2015). Motor performance of children with Down syndrome and typical development at 2 to 4 and 26 months. *Pediatr Phys Ther* **27**, 135-141.

Chang, P., Bush, D., Schorge, S., Good, M., Canonica, T., Shing, N., Noy, S., Wiseman, F. K., Burgess, N., Tybulewicz, V. L. J., et al. (2020). Altered Hippocampal-Prefrontal Neural Dynamics in Mouse Models of Down Syndrome. *Cell Rep* **30**, 1152-1163.

Costa, R., Gullon, A., De Miguel, R., de Asua, D. R., Bautista, A., Garcia, C., Suarez, C., Castaneda, S. and Moldenhauer, F. (2018). Bone Mineral Density Distribution Curves in Spanish Adults With Down Syndrome. *J Clin Densitom* **21**, 493-500.

Fernhall, B. and Otterstetter, M. (2003). Attenuated responses to sympathoexcitation in individuals with Down syndrome. *J Appl Physiol* **94**, 2158-2165.

Garnett, C., Cruz Hernandez, D. and Vyas, P. (2020). GATA1 and cooperating mutations in myeloid leukaemia of Down syndrome. *IUBMB Life* **72**, 119-130.

Goodliffe, J. W., Olmos-Serrano, J. L., Aziz, N. M., Pennings, J. L., Guedj, F., Bianchi, D. W. and Haydar, T. F. (2016). Absence of Prenatal Forebrain Defects in the Dp(16)1Yey/+ Mouse Model of Down Syndrome. *J Neurosci* **36**, 2926-2944.

Grieco, J., Pulsifer, M., Seligsohn, K., Skotko, B. and Schwartz, A. (2015). Down syndrome: Cognitive and behavioral functioning across the lifespan. *Am J Med Genet C Semin Med Genet* **169**, 135-149.

Gutierrez-Hervas, A., Gomez-Martinez, S., Izquierdo-Gomez, R., Veiga, O. L., Perez-Bey, A., Castro-Pinero, J. and Marcos, A. (2020). Inflammation and fatness in adolescents with and without Down syndrome: UP & DOWN study. *J Intellect Disabil Res* **64**, 170-179.

Iellamo, F., Galante, A., Legramante, J. M., Lippi, M. E., Condoluci, C., Albertini, G. and Volterrani, M. (2005). Altered autonomic cardiac regulation in individuals with Down syndrome. *Am J Physiol Heart Circ Physiol* **289**, H2387-2391.

Jiang, X., Liu, C., Yu, T., Zhang, L., Meng, K., Xing, Z., Belichenko, P. V., Kleschevnikov, A. M., Pao, A., Peresie, J., et al. (2015). Genetic dissection of the Down syndrome critical region. *Hum Mol Genet* **24**, 6540-6551.

Johnson, M. B., De Franco, E., Greeley, S. A. W., Letourneau, L. R., Gillespie, K. M., International, D. S. P. C., Wakeling, M. N., Ellard, S., Flanagan, S. E., Patel, K. A., et al. (2019). Trisomy 21 Is a Cause of Permanent Neonatal Diabetes That Is Autoimmune but Not HLA Associated. *Diabetes* **68**, 1528-1535.

Korenberg, J. R., Chen, X. N., Schipper, R., Sun, Z., Gonsky, R., Gerwehr, S., Carpenter, N., Daumer, C., Dignan, P., Disteche, C., et al. (1994). Down syndrome phenotypes: the consequences of chromosomal imbalance. *Proc Natl Acad Sci U S A* **91**, 4997-5001.

Kreicher, K. L., Weir, F. W., Nguyen, S. A. and Meyer, T. A. (2018). Characteristics and Progression of Hearing Loss in Children with Down Syndrome. *J Pediatr* **193**, 27-33 e22.

Krinsky-McHale, S. J., Silverman, W., Gordon, J., Devenny, D. A., Oley, N. and Abramov, I. (2014). Vision deficits in adults with Down syndrome. *J Appl Res Intellect Disabil* **27**, 247-263.

LaCombe, J. M. and Roper, R. J. (2020). Skeletal dynamics of Down syndrome: A developing perspective. *Bone* **133**, 115215.

Laguna, A., Barallobre, M. J., Marchena, M. A., Mateus, C., Ramirez, E., Martinez-Cue, C., Delabar, J. M., Castelo-Branco, M., de la Villa, P. and Arbones, M. L. (2013). Triplication of DYRK1A causes retinal structural and functional alterations in Down syndrome. *Hum Mol Genet* **22**, 2775-2784.

Lana-Elola, E., Watson-Scales, S., Slender, A., Gibbins, D., Martineau, A., Douglas, C., Mohun, T., Fisher, E. M. and Tybulewicz, V. (2016). Genetic dissection of Down

syndrome-associated congenital heart defects using a new mouse mapping panel. *Elife* **5**, 10.7554/eLife.11614.

Levenga, J., Peterson, D. J., Cain, P. and Hoeffer, C. A. (2018). Sleep Behavior and EEG Oscillations in Aged Dp(16)1Yey/+ Mice: A Down Syndrome Model. *Neuroscience* **376**, 117-126.

Li, Z., Yu, T., Morishima, M., Pao, A., LaDuca, J., Conroy, J., Nowak, N., Matsui, S., Shiraishi, I. and Yu, Y. E. (2007). Duplication of the entire 22.9-Mb human chromosome 21 syntenic region on mouse chromosome 16 causes cardiovascular and gastrointestinal abnormalities. *Hum Mol Genet* **16**, 1359-1366.

Liu, C., Morishima, M., Yu, T., Matsui, S. I., Zhang, L., Fu, D., Pao, A., Costa, A. C., Gardiner, K. J., Cowell, J. K., et al. (2011). Genetic analysis of Down syndrome-associated heart defects in mice. *Hum Genet*.

Liu, C., Yu, T., Xing, Z., Jiang, X., Li, Y., Pao, A., Mu, J., Wallace, P. K., Stoica, G., Bakin, A. V., et al. (2018). Triplications of human chromosome 21 orthologous regions in mice result in expansion of megakaryocyte-erythroid progenitors and reduction of granulocyte-macrophage progenitors. *Oncotarget* **9**, 4773-4786.

Lott, I. T. and Dierssen, M. (2010). Cognitive deficits and associated neurological complications in individuals with Down's syndrome. *Lancet Neurol* **9**, 623-633.

Luke, A., Roizen, N. J., Sutton, M. and Schoeller, D. A. (1994). Energy expenditure in children with Down syndrome: correcting metabolic rate for movement. *J Pediatr* **125**, 829-838.

Malak, R., Kostiukow, A., Krawczyk-Wasielewska, A., Mojs, E. and Samborski, W. (2015). Delays in Motor Development in Children with Down Syndrome. *Med Sci Monit* **21**, 1904-1910.

Menzies, C., Naz, S., Patten, D., Alquier, T., Bennett, B. M. and Lacoste, B. (2021). Distinct Basal Metabolism in Three Mouse Models of Neurodevelopmental Disorders. *eNeuro* **8**.

Nguyen, T. L., Duchon, A., Manousopoulou, A., Loaec, N., Villiers, B., Pani, G., Karatas, M., Mechling, A. E., Harsan, L. A., Limanton, E., et al. (2018). Correction of cognitive deficits in mouse models of Down syndrome by a pharmacological inhibitor of DYRK1A. *Dis Model Mech* **11**.

Patel, A., Yamashita, N., Ascano, M., Bodmer, D., Boehm, E., Bodkin-Clarke, C., Ryu, Y. K. and Kuruvilla, R. (2015). RCAN1 links impaired neurotrophin trafficking to aberrant development of the sympathetic nervous system in Down syndrome. *Nat Commun* **6**, 10119.

Peiris, H., Duffield, M. D., Fadista, J., Jessup, C. F., Kashmir, V., Genders, A. J., McGee, S. L., Martin, A. M., Saiedi, M., Morton, N., et al. (2016). A Syntenic Cross Species Aneuploidy Genetic Screen Links RCAN1 Expression to beta-Cell Mitochondrial Dysfunction in Type 2 Diabetes. *PLoS Genet* **12**, e1006033.

Pinto, B., Morelli, G., Rastogi, M., Savardi, A., Fumagalli, A., Petretto, A., Bartolucci, M., Varea, E., Catelani, T., Contestabile, A., et al. (2020). Rescuing Over-activated Microglia Restores Cognitive Performance in Juvenile Animals of the Dp(16) Mouse Model of Down Syndrome. *Neuron*.

Raveau, M., Polygalov, D., Boehringer, R., Amano, K., Yamakawa, K. and McHugh, T. J. (2018). Alterations of in vivo CA1 network activity in Dp(16)1Yey Down syndrome model mice. *Elife* **7**, 10.7554/eLife.31543.

Souchet, B., Duchon, A., Gu, Y., Dairou, J., Chevalier, C., Daubigney, F., Nalesso, V., Creau, N., Yu, Y., Janel, N., et al. (2019). Prenatal treatment with EGCG enriched green tea extract rescues GAD67 related developmental and cognitive defects in Down syndrome mouse models. *Sci Rep* **9**, 3914.

Starbuck, J. M., Dutka, T., Ratliff, T. S., Reeves, R. H. and Richtsmeier, J. T. (2014). Overlapping trisomies for human chromosome 21 orthologs produce similar effects on skull and brain morphology of Dp(16)1Yey and Ts65Dn mice. *Am J Med Genet A* **164A**, 1981-1990.

Sullivan, K. D., Lewis, H. C., Hill, A. A., Pandey, A., Jackson, L. P., Cabral, J. M., Smith, K. P., Liggett, L. A., Gomez, E. B., Galbraith, M. D., et al. (2016). Trisomy 21 consistently activates the interferon response. *Elife* **5**.

Takahashi, T., Sakai, N., Iwasaki, T., Doyle, T. C., Mobley, W. C. and Nishino, S. (2020). Detailed evaluation of the upper airway in the Dp(16)1Yey mouse model of Down syndrome. *Sci Rep* **10**, 21323.

Thomas, J. R., LaCombe, J., Long, R., Lana-Elola, E., Watson-Scales, S., Wallace, J. M., Fisher, E. M. C., Tybulewicz, V. L. J. and Roper, R. J. (2020). Interaction of sexual dimorphism and gene dosage imbalance in skeletal deficits associated with Down syndrome. *Bone* **136**, 115367.

Toussaint, N., Redhead, Y., Vidal-Garcia, M., Lo Vercio, L., Liu, W., Fisher, E. M. C., Hallgrímsson, B., Tybulewicz, V. L. J., Schnabel, J. A. and Green, J. B. A. (2021). A landmark-free morphometrics pipeline for high-resolution phenotyping: application to a mouse model of Down Syndrome. *Development* **148**, dev188631.

Vicente, A., Bravo-Gonzalez, L. A., Lopez-Romero, A., Munoz, C. S. and Sanchez-Meca, J. (2020). Craniofacial morphology in down syndrome: a systematic review and meta-analysis. *Sci Rep* **10**, 19895.

Victorino, D. B., Scott-McKean, J. J., Johnson, M. W. and Costa, A. C. S. (2020). Quantitative Analysis of Retinal Structure and Function in Two Chromosomally Altered Mouse Models of Down Syndrome. *Invest Ophthalmol Vis Sci* **61**, 25.

Vis, J. C., Duffels, M. G., Winter, M. M., Weijerman, M. E., Cobben, J. M., Huisman, S. A. and Mulder, B. J. (2009). Down syndrome: a cardiovascular perspective. *J Intellect Disabil Res* **53**, 419-425.

Watson-Scales, S., Kalmar, B., Lana-Elola, E., Gibbins, D., La Russa, F., Wiseman, F., Williamson, M., Saccon, R., Slender, A., Olerinyova, A., et al. (2018). Analysis of motor dysfunction in Down Syndrome reveals motor neuron degeneration. *PLoS Genet* **14**, e1007383.

Wiseman, F. K., Al-Janabi, T., Hardy, J., Karmiloff-Smith, A., Nizetic, D., Tybulewicz, V. L., Fisher, E. M. and Strydom, A. (2015). A genetic cause of Alzheimer disease: mechanistic insights from Down syndrome. *Nat Rev Neurosci* **16**, 564-574.

Yu, T., Clapcote, S. J., Liu, C., Li, S., Pao, A., Bechard, A. R., Belichenko, P., Kleschevnikov, A., Asrar, S., Chen, R., et al. (2010). Effects of individual segmental trisomies of human chromosome 21 syntenic regions on hippocampal long-term potentiation and cognitive behaviors in mice. *Brain Res* **1366**, 162-171.

Zhang, L., Meng, K., Jiang, X., Liu, C., Pao, A., Belichenko, P. V., Kleschevnikov, A. M., Josselyn, S., Liang, P., Ye, P., et al. (2014). Human chromosome 21 orthologous region on mouse chromosome 17 is a major determinant of Down syndrome-related developmental cognitive deficits. *Hum Mol Genet* **23**, 578-589.